Efficient algorithm for multiconfiguration pair-density functional theory with application to the heterolytic dissociation energy of ferrocene

Andrew M. Sand, Donald G. Truhlar,[a] and Laura Gagliardi[a]
Department of Chemistry, Chemical Theory Center, and Supercomputing Institute, University of Minnesota, Minneapolis, Minnesota 55455-0431, USA

(Received 4 October 2016; accepted 23 December 2016; published online 17 January 2017)

The recently developed multiconfiguration pair-density functional theory (MC-PDFT) combines multiconfiguration wave function theory with a density functional that depends on the on-top pair density of an electronic system. In an MC-PDFT calculation, there are two steps: a conventional multiconfiguration self-consistent-field (MCSCF) calculation and a post-MCSCF evaluation of the energy with an on-top density functional. In this work, we present the details of the MC-PDFT algorithm that avoids steeply scaling steps that are present in other post-self-consistent-field multireference calculations of dynamic correlation energy. We demonstrate the favorable scaling by considering systems of H_2 molecules with active spaces of several different sizes. We then apply the MC-PDFT method to calculate the heterolytic dissociation enthalpy of ferrocene. We find that MC-PDFT yields results that are at least as accurate as complete active space second-order perturbation theory and are more stable with respect to basis set, but at a fraction of the cost in both time and memory. *Published by AIP Publishing.* [http://dx.doi.org/10.1063/1.4973709]

I. INTRODUCTION

Descriptions of chemical systems by quantum mechanical methods require a balance between accuracy and cost in the treatment of correlation energy.[1–7] Kohn-Sham density functional theory (KS-DFT) provides the best balance for many large and complex systems, but because it calculates the kinetic energy and spin densities from a single Slater determinant, its accuracy with available density functionals is sometimes low for systems with high static correlation.[8] An alternative approach for such systems is to use multireference wave function methods,[1–3,6–12] but the cost of this approach scales poorly with system size, making its application to many interesting systems limited or impractical.

Multiconfiguration pair-density functional theory (MC-PDFT)[13] is a relatively new kind of density functional theory in which the electronic energy is calculated from the kinetic energy, density, and the on-top pair density of a multiconfiguration wave function. The MC-PDFT method requires a reference calculation to generate an on-top pair density, which is the probability of finding two electrons at a given point in space. In general, any method that generates a two-body density matrix can be used as an MC-PDFT reference, although so far applications have been limited to multiconfigurational self-consistent field (MCSCF) wave functions, for which one may view MC-PDFT as a post-MCSCF method.

Post-MCSCF methods, including MC-PDFT, consist of two parts: (i) an initial MCSCF calculation, which is usually designed primarily to yield suitable orbitals for the next step and to account for static electron correlation but which also inevitably includes some dynamic correlation, and (ii) a post-SCF step to calculate the final energy.

In several applications of MC-PDFT to date, the initial MCSCF calculation (step (i)) has been a complete active space self-consistent field (CASSCF)[1–3] calculation; whereas in others it has been a generalized active space self-consistent field (GASSCF)[14] calculation. Standard CASSCF techniques are limited by computational costs to modest-sized systems, for example, for closed-shell singlets, to the treatment of no more than approximately 18 electrons in 18 active orbitals, but the treatment of larger active spaces is possible through the use of GASSCF or other MCSCF methods, including restricted active space self-consistent field (RASSCF),[15] occupation-restricted multiple active space (ORMAS),[16] splitGAS,[17,18] stochastic CASSCF approaches,[19] density matrix renormalization group (DMRG),[20–22] and the variational 2-RDM method.[23–25]

One kind of post-SCF correction (step (ii)) is multireference second-order perturbation theory (MR-PT2), which can be used with a number of reference wave functions including CASSCF, which yields CASPT2,[26] RASSCF, which yields RASPT2,[27] and GASSCF, which yields GASPT2.[28] Another kind of post-SCF treatment, which is the main subject of the present paper, is MC-PDFT. The MR-PT2 and MC-PDFT methods have different dependencies on the two-, three-, and four-body density matrices of the reference wave function. The MC-PDFT method requires only the two-body density matrix of the reference wave function, and the size of this matrix scales as the size of the active space to the fourth power. The solution to the MR-PT2 equations requires up to the four-body density matrix, and the size of this matrix scales as the size of the active space to the eighth power. This dependence on higher-order density matrices imposes two constraints on the MR-PT2 method. First, the three- and four-body density matrices are not generally readily available from the reference

[a] Authors to whom correspondence should be addressed. Electronic addresses: truhlar@umn.edu and gagliardi@umn.edu

calculation, and they must be constructed from the reference wave function as an additional post-SCF step. The construction of the higher-order density matrices from the CI expansion coefficients scales exponentially with the active space size; this results in an active space limit of about 16 electrons in 16 active orbitals for CASPT2, which is slightly more restrictive than the size limitations on the CASSCF reference wave function. MC-PDFT, on the other hand, does not require the construction of any density matrices of order higher than 2, and this means that MC-PDFT calculations are computationally limited only by the reference calculation limitations. Restrictions on the CI expansion of the wave function, as employed for RASSCF, GASSCF, and ORMAS, enable the treatment of larger active spaces. As the active space grows, one eventually encounters the second constraint, which is that the handling of the four-body density matrix, which is required for CASPT2, RASPT2, and GASPT2 calculations, is not practical for more than about 30 active orbitals. If one wants to use one of these large-active space wave functions as a reference in conjunction with perturbative techniques, alternative forms of perturbation theory must be used, such as strongly contracted *n*-electron valence perturbation theory.[29,30] There is no such limitation for MC-PDFT—if the reference calculation can be performed to generate the two-body density matrix, an MC-PDFT calculation can also be performed. Other methods that have been suggested for overcoming these computational limitations are range-separated multireference density functional theory[36–39] and using a pair coupled cluster doubles reference in conjunction with an on-top pair density functional.[40]

MC-PDFT with a CASSCF reference function has been shown to give good results for barrier heights and main-group and transition-metal energetics[31] and excited states.[32–34] MC-PDFT has also been shown[35] to work well with a low-cost separated-pair reference wave function, which is a special case of GASSCF. In the present paper, we present the structure of the MC-PDFT algorithm in order to give a clear understanding of how an MC-PDFT calculation can be performed and to show how the scaling of MC-PDFT calculations provides a significant advantage in application to large-active-space calculations. For simplicity we only explicitly consider the case of a CASSCF wave function, but the algorithm and most of the considerations are more general and apply to other types of MCSCF reference functions. We will give examples of the costs of these calculations in terms of both time and memory for systems of hydrogen molecules separated by 20 Å with a variety of active space sizes. We will compare the scaling results to those obtained via CASSCF and CASPT2. We also present calculations of the heterolytic dissociation enthalpy of ferrocene in order to illustrate the accuracy of MC-PDFT for systems with large active spaces.

The dissociation enthalpy of ferrocene has been the subject both experimental[41] and computational[42–50] studies. This problem requires being able to describe two spin states in a consistent fashion. The ground state of ferrocene is a singlet state whereas the dissociated molecule consists of a quintet-state Fe^{2+} atom and two singlet-state cyclopentadienyl anion ligands. Furthermore, one must use large basis sets and large active spaces in order to obtain results that agree with experiment.[43,48] Thus it is interesting to test whether MC-PDFT is useful for studying this kind of system.

II. THEORY

A. MC-PDFT theory

In MC-PDFT, we express the energy as

$$E = V_{\rm nn} + \left\langle \Psi | \hat{T} + \hat{V}_{\rm ne} | \Psi \right\rangle + V_{\rm C}[\rho(\boldsymbol{r})] + E_{\rm ot}[\rho(\boldsymbol{r}), \Pi(\boldsymbol{r})], \tag{1}$$

where $V_{\rm nn}$ is the nuclear repulsion, Ψ is a multiconfigurational wave function, $\hat{T}$ is the kinetic energy operator, $\hat{V}_{\rm ne}$ is the nuclear-electron interaction operator, $V_{\rm C}[\rho(\boldsymbol{r})]$ is the classical electrostatic energy, and $E_{\rm ot}[\rho(\boldsymbol{r}), \Pi(\boldsymbol{r})]$ is the on-top density functional, which depends on the electronic density $\rho(\boldsymbol{r})$ and the on-top pair density $\Pi(\boldsymbol{r})$. The density and on-top pair density can be expressed as (we assume real orbitals to keep the notation simple)

$$\rho(\boldsymbol{r}) = \sum_{pq} \phi_p(\boldsymbol{r}) \phi_q(\boldsymbol{r}) D_{pq}, \tag{2}$$

$$\Pi(\boldsymbol{r}) = \sum_{pqst} \phi_p(\boldsymbol{r}) \phi_q(\boldsymbol{r}) \phi_s(\boldsymbol{r}) \phi_t(\boldsymbol{r}) d_{pqst}, \tag{3}$$

where $\phi_i(\boldsymbol{r})$ are orbitals, and D_{pq} and d_{pqst} are the one- and two-body density matrices, respectively. We can rewrite Eq. (1) in terms of the one- and two-electron integrals and density matrices,

$$E = V_{nn} + \sum_{pq} h_{pq} D_{pq} + \frac{1}{2} \sum_{pqst} g_{pqst} D_{pq} D_{st} + E_{\rm ot}[\rho(\boldsymbol{r}), \Pi(\boldsymbol{r})], \tag{4}$$

where h_{pq} and g_{pqst} are the one- and two-electron integrals,

$$h_{pq} = \int \phi_p^*(\boldsymbol{r}) h(\boldsymbol{r}) \phi_q(\boldsymbol{r}) d\boldsymbol{r}, \tag{5}$$

$$g_{pqst} = \int\int \phi_s^*(\boldsymbol{r}_1) \phi_t(\boldsymbol{r}_1) \frac{1}{|\boldsymbol{r}_1 - \boldsymbol{r}_2|} \phi_p^*(\boldsymbol{r}_2) \phi_q(\boldsymbol{r}_2) d\boldsymbol{r}_1 d\boldsymbol{r}_2, \tag{6}$$

and the one-electron operator $h(\boldsymbol{r})$ includes both electronic kinetic energy and electron-nuclear potential energy,

$$h(\boldsymbol{r}) = \frac{-\nabla^2}{2} - \sum_A \frac{Z_A}{|\boldsymbol{r} - \boldsymbol{r}_A|}. \tag{7}$$

Thus in MC-PDFT, the one-electron and classical electrostatic energies are taken directly from the MCSCF wave function, and the remaining energy is calculated via the on-top pair density functional.

If in Eq. (1) we restrict Ψ to be a single Slater determinant (Ψ_s) and if we replace the on-top energy functional by an exchange-correlation functional $E_{\rm xc}[\rho(\boldsymbol{r})]$, we obtain the KS energy expression,

$$E_{\rm KS-DFT} = V_{\rm nn} + \left\langle \Psi_s | \hat{T} + \hat{V}_{\rm ne} | \Psi_s \right\rangle + V_{\rm C}[\rho(\boldsymbol{r})] + E_{\rm xc}[\rho(\boldsymbol{r})]. \tag{8}$$

Similarly, Eq. (4) becomes the MCSCF energy expression upon the inclusion of all two-body density matrix terms and dropping the on-top pair density functional,

$$E_{\mathrm{MCSCF}} = V_{\mathrm{nn}} + \sum_{pq} h_{pq} D_{pq} + \frac{1}{2} \sum_{pqst} g_{pqst} d_{pqst}. \tag{9}$$

The on-top energy functionals that we have employed in Eq. (1) are generated by translating existing generalized gradient approximation density functionals.[13] These functionals depend on the total density ρ and the spin magnetization density m, which are expressible in terms of the spin-up and spin-down electron densities ρ_α and ρ_β as

$$\rho(\boldsymbol{r}) = \rho_\alpha(\boldsymbol{r}) + \rho_\beta(\boldsymbol{r}), \tag{10}$$

$$m(\boldsymbol{r}) = \rho_\alpha(\boldsymbol{r}) - \rho_\beta(\boldsymbol{r}), \tag{11}$$

and additionally depend on the gradients of $\rho'(\boldsymbol{r})$ and $m'(\boldsymbol{r})$,

$$\rho'(\boldsymbol{r}) = \rho'_\alpha(\boldsymbol{r}) + \rho'_\beta(\boldsymbol{r}), \tag{12}$$

$$m'(\boldsymbol{r}) = \rho'_\alpha(\boldsymbol{r}) - \rho'_\beta(\boldsymbol{r}). \tag{13}$$

Given a KS density functional $E_{\mathrm{xc}}[\rho, m, \rho', m']$, the translation scheme we use is defined as[13]

$$E_{\mathrm{ot}}[\rho(\boldsymbol{r}), \Pi(\boldsymbol{r})] = E_{\mathrm{xc}}\left[\rho(\boldsymbol{r}), \begin{Bmatrix} \rho(\boldsymbol{r})(1-R)^{1/2} & \text{if } R(\boldsymbol{r}) \le 1 \\ 0 & \text{if } R(\boldsymbol{r}) > 1 \end{Bmatrix}, \rho'(\boldsymbol{r}), \begin{Bmatrix} \rho'(\boldsymbol{r})(1-R)^{1/2} & \text{if } R(\boldsymbol{r}) \le 1 \\ 0 & \text{if } R(\boldsymbol{r}) > 1 \end{Bmatrix}\right], \tag{14}$$

where

$$R(\boldsymbol{r}) = \frac{\Pi(\boldsymbol{r})}{[\rho(\boldsymbol{r})/2]^2}. \tag{15}$$

Equivalently, by using Eqs. (10)–(13), we can express the translation scheme in terms of α-spin and β-spin translated densities $\tilde{\rho}$ and density gradients $\tilde{\rho}'$,

$$\tilde{\rho}_\alpha(\boldsymbol{r}) = \begin{cases} \left(\rho(\boldsymbol{r})/2\right)\left(1+\sqrt{1-R(\boldsymbol{r})}\right) & \text{if } R(\boldsymbol{r}) \le 1 \\ \left(\rho(\boldsymbol{r})/2\right) & \text{if } R(\boldsymbol{r}) > 1 \end{cases}, \tag{16}$$

$$\tilde{\rho}_\beta(\boldsymbol{r}) = \begin{cases} \left(\rho(\boldsymbol{r})/2\right)\left(1-\sqrt{1-R(\boldsymbol{r})}\right) & \text{if } R(\boldsymbol{r}) \le 1 \\ \left(\rho(\boldsymbol{r})/2\right) & \text{if } R(\boldsymbol{r}) > 1 \end{cases}, \tag{17}$$

$$\tilde{\rho}'_\alpha(\boldsymbol{r}) = \begin{cases} \left(\rho'(\boldsymbol{r})/2\right)\left(1+\sqrt{1-R(\boldsymbol{r})}\right) & \text{if } R(\boldsymbol{r}) \le 1 \\ \left(\rho'(\boldsymbol{r})/2\right) & \text{if } R(\boldsymbol{r}) > 1 \end{cases}, \tag{18}$$

$$\tilde{\rho}'_\beta(\boldsymbol{r}) = \begin{cases} \left(\rho'(\boldsymbol{r})/2\right)\left(1-\sqrt{1-R(\boldsymbol{r})}\right) & \text{if } R(\boldsymbol{r}) \le 1 \\ \left(\rho'(\boldsymbol{r})/2\right) & \text{if } R(\boldsymbol{r}) > 1 \end{cases}. \tag{19}$$

B. MC-PDFT algorithm

The general algorithm for the computation of the MC-PDFT energy is given in Figure 1. The MC-PDFT energy calculation involves three tasks: (i) an initial MCSCF calculation to generate the one- and two-body density matrices, (ii) the evaluation of the energy contribution from the on-top density functional, and (iii) the evaluation of the energy contribution that comes from the MCSCF wave function. Task (iii) includes the kinetic energy, the electron-nuclear potential energy, and the electron-electron classical electrostatic potential energy.

In the rest of the development we call the basis functions the AOs, and we call the self-consistent orbitals obtained by solving the MCSCF equations the molecular orbitals (MOs).

To begin, one calculates a set of molecular orbitals (MOs) and the one- and two-body density matrices in the MO basis (task (i)). The orbitals in an MCSCF wave function can be partitioned into three sets: inactive (doubly occupied), active (variably occupied), and virtual (unoccupied). Next, one calculates the contribution to the energy from the on-top density functional (task (ii)). This proceeds in a manner similar to the way that the density functional is evaluated in KS density functional theory, i.e., the on-top functional is evaluated numerically on a grid. As in KS density functional theory, the on-top functional requires the value of the one-electron density at each grid point $\boldsymbol{r}$, evaluated by multiplying the one-body density matrix in the AO basis by the values of the basis functions evaluated on the grid,

$$\rho(\boldsymbol{r}) = \sum_{pq} \chi_p(\boldsymbol{r}) \chi_q(\boldsymbol{r}) D_{pq}, \tag{20}$$

where χ_p is a basis function. Unlike KS density functional theory, MC-PDFT also requires the on-top pair density at each grid point. The on-top pair density requires the two-body density matrix, as seen in Eq. (3).

After a standard MCSCF calculation, the two-body density matrix is available in the MO basis; however in Eq. (20) only the AOs have been evaluated on the grid. Therefore, in order to obtain the on-top pair density, one must either transform the two-body density matrix to the AO basis or evaluate the molecular orbitals at each of the grid points. The number of nonzero elements in the two-body density matrix in the MO basis scales as the number of active orbitals to the fourth power, but the number of elements in the two-body density matrix in the AO basis scales as the number of atomic orbitals to the fourth power, and therefore transformation of the density matrix requires very large storage when the number of basis functions is large. For this reason, we choose to evaluate the MOs on the grid.

Following the calculation of the on-top pair density at each grid point, we proceed with the determination of the translated densities $\tilde{\rho}$ and density gradients $\nabla\tilde{\rho}$ using Eqs. (16)–(19). The translated components $\tilde{\rho}$ and $\nabla\tilde{\rho}$ are then passed to the KS density functional theory kernel to determine the on-top energy contribution given by

$$E_{\mathrm{ot}} = \int F[\tilde{\rho}(\boldsymbol{r}), \nabla\tilde{\rho}(\boldsymbol{r})]\tilde{\rho}(\boldsymbol{r})\, d\boldsymbol{r}. \tag{21}$$

1: **procedure** Reference Calculation
2: Obtain one-body density matrices (*D*), two-body density matrices (*d*), MO coefficients, one-and two-electron integrals
3: **procedure** MC-PDFT Energy Calculation
4: **procedure** Calculation of on-top energy contribution
5: Read *d* and *D* (MO basis)
6: Transform *d* to AO basis
7: Define grid, parse into batches of grid points
8: **for** each batch of grid points **do**
9: Calculate the value of each AO and MO at the grid points
10: Calculate ρ at the grid points
11: **if** functional is of GGA type **then**
12: Calculate AO and MO gradients at the grid points
13: Calculate the gradient of ρ at the grid points
14: **for** MOs *pqrs* **do**
15: **for** each grid point in the batch **do**
16: Calculate on-top density at the grid point
17: **if** functional is of GGA type **then**
18: Calculate on-top density gradient at the grid point
19: **for** each grid point in the batch **do**
20: Translate densities ρ_α, ρ_β
21: **if** functional is of GGA type **then**
22: Translate gradients $\nabla\rho_\alpha$, $\nabla\rho_\beta$ at the grid point
23: Calculate the density functional contribution to the energy from the batch and accumulate
24: **procedure** Calculation of CASSCF Energy Contribution
25: Transform AO integrals to the inactive-inactive, inactive-active, and active-active subsets of MO integrals
26: Replace the two-body density matrix elements *dpqrs* with a product of one-body matrix elements *DpqDrs*
27: Assemble Fock matrix components F^{I} and F^{A}
28: Determine CASSCF energy contribution using existing CASSCF routines and the calculated Fock matrix.
29: Combine energies of steps 23 and 28 to obtain MC-PDFT energy

FIG. 1. Algorithm for the determination of the MC-PDFT energy.

Next the energy contribution from the MCSCF wave function is considered (task (iii)). Here we use the indices t, u, v, and x to indicate active orbitals, i and j to indicate inactive orbitals, and p and q to indicate active or inactive orbitals. An integral transformation of the one- and two-electron integrals from the AO basis to the MO basis is performed. As can be seen in Eq. (4), only those integrals that are multiplied by nonzero density matrix elements can contribute to the energy. Thus, our integral transformation can be limited to the generation of h_{ii} and h_{tu} one-electron integrals as well as $(ii|jj)$ and $(tu|vx)$ two-electron integrals. These integrals are a subset of the integrals needed in the calculation of the MCSCF energy. The energy contribution is computed efficiently using the existing MCSCF routines with a few modifications. In particular we calculate the MCSCF energy contribution by modifying the Fock operator formalism used in conventional MCSCF calculations:[51] (1) the exchange contribution to the Fock operator is omitted; (2) the two-body density matrix is replaced element-by-element with a product of elements of the one-body density matrix (line 26 of Figure 1). The energy contribution from the MCSCF portion of the calculation is calculated as

$$E_{\mathrm{MCSCF}} = E_{\mathrm{nn}} + \sum_i D_{ii}F^{\mathrm{I}}_{ii} + \sum_{pq}\left(F^{\mathrm{I}}_{pq} + \frac{1}{2}F^{\mathrm{A}}_{pq}\right)D_{pq}, \tag{22}$$

where E_{nn} is the nuclear repulsion energy and F^I and F^A are the inactive-Fock and active-Fock matrices, respectively,

$$F^{\mathrm{I}}_{pq} = h_{pq} + 2\sum_j (pq|jj), \tag{23}$$

$$F^{\mathrm{A}}_{pq} = \sum_{tu} D_{tu}(pq|tu). \tag{24}$$

As previously stated, in MC-PDFT calculations, the limitations due to computer time and memory are due to the portions of the calculation involving the two-body density matrix. The MC-PDFT algorithm we present requires the storage of the two-body density matrix, spanning the active orbital subspace, and the evaluation of on-top density and its gradient scales with the number of elements in this matrix. Because the two-body density matrix scales modestly as N^4 with the number of active orbitals, active space sizes of 50 orbitals or more are not problematic for the post-SCF portion of the calculation. In order to realize calculations on active space systems of this size, however, one must employ an MCSCF method for which large active spaces are feasible.

III. COMPUTATIONAL DETAILS

All MC-PDFT calculations that we present use a CASSCF reference wave function; thus, we identify these calculations as CAS-PDFT. All KS density functional theory (KS-DFT), CASSCF, CASPT2, and CAS-PDFT calculations in this article were performed using a locally modified version of *Molcas* 8.1.[6] All CAS-PDFT calculations used the tPBE on-top density functional,[13] which is a translation of the PBE exchange-correlation functional from KS density functional theory. All calculations were performed using a single CPU.

A. Separated H_2 molecules

Calculations on systems of H_2 molecules (20 Å apart) were performed using the cc-pVQZ basis set;[52] one to eight molecules were used. Each H_2 molecule contributes two electrons and two orbitals to the active space, making the total active space $(2n, 2n)$ for a system of n H_2 molecules.

B. Ferrocene dissociation energy

The structure used for the ferrocene molecule was taken from previous work,[43] in which geometry optimization was performed using CCSD(T)/TZV2P+f. For the Cp^- ligand, we calculated the structure by geometry optimization using CCSD(T)[53]/TZV2P[54] with D_{5h} symmetry, employing the GAMESS electronic structure package.[1,56] The second-order Douglas-Kroll-Hess Hamiltonian[55] was used for all calculations in combination with an all-electron

relativistic basis set in order to include scalar relativistic effects.

Four different basis sets were used. The smallest basis set consists of the cc-pVDZ-DK[52] basis for C and H atoms and the cc-pVTZ-DK[52,57,58] basis for the Fe atom. We next added diffuse functions through the use of minimally augmented correlation-consistent (maug-cc) basis sets,[59,60] which augment the correlation-consistent basis functions[52,57,58] with s and p diffuse functions on the non-hydrogen atoms. The maug-cc-pVDZ-DK basis was used for C and H atoms, and the maug-cc-pVTZ-DK basis was used for the Fe atom. We also employed larger basis sets, employing cc-pVTZ-DK for C and H atoms and cc-pVQZ for the Fe atom. We further employed the minimally augmented forms of these bases as well, using the maug-cc-pVTZ-DK basis for C and H atoms and the maug-cc-pVQZ-DK basis for Fe.

Cholesky decomposition via resolution-of-the-identity[61] was used for all calculations, using a threshold of 10^{-8} a.u.

For each molecule or fragment, the same active space was used for the CASSCF, CASPT2, and CAS-PDFT calculations. The 1s orbital of each carbon atom and the 1s, 2s, and 2p orbitals of the iron atom were frozen (not correlated) for the CASPT2 calculations. We used C_1 symmetry for all calculations; however, we label the orbitals according to their D_{5h} point-group designations. A (14,14) active space was selected for the ferrocene molecule; the orbitals are shown in Figure 2. This active space was formed by taking the (10,10) active space previously suggested for CASPT2 calculations,[42,49] which includes the $a_1'(3d_{z^2})$, $a_1'(4d_{z^2})$, $e_1''(3d_{xz}, 3d_{yz})$, and $e_2'(3d_{xy}, 3d_{x^2-y^2})$ orbitals of primarily metal-orbital character, plus the $e_2'(\pi^*)$ and $e_1''(\pi)$ orbitals of primarily ligand character. We added four additional ligand orbitals, ($e_1'(\pi)$ and $e_2''(\pi^*)$), to bring the entire ligand π-system into the active space with the exception of the lowest-lying a_1' orbital which is energetically separated from the metal d orbitals. Because the ligand orbitals $e_2'(\pi^*)$ and $e_1''(\pi)$ include a mix of metal d orbitals, we have not included additional correlating 4d orbitals beyond the $a_1'(4d_{z^2})$ already specified. For active-space consistency between the bound $FeCp_2$ molecule and the unbound metal and ligand fragments, we use a (6,6) active space on the Fe^{2+} fragment and a (4,4) active space on each of the Cp^- fragments.

The binding energy of ferrocene is calculated as

$$D_e = E\left(Fe^{2+}\right) + 2E\left(Cp^-\right) - E(FeCp_2). \tag{25}$$

To obtain the dissociation enthalpy, we must also account for zero-point energy (ZPE) and thermal contributions; these are taken from a previous reference,[49] where they were determined from frequency calculations using PBE0 with the def2-TZVP basis for C and H atoms and the def2-QZVPP basis for the Fe atom. Additionally, one may consider adding a correction for basis set superposition error (BSSE); this is done using a counterpoise correction (CPC).[62,63] For small basis sets, it is often observed that the standard CPC results in binding and dissociation energies that are too low. Several authors have advocated scaling the CPC by one-half to obtain more accurate results.[64–66] We will consider three possible options: no CPC, full CPC (denoted CPC-f), and one-half CPC (denoted CPC/2).

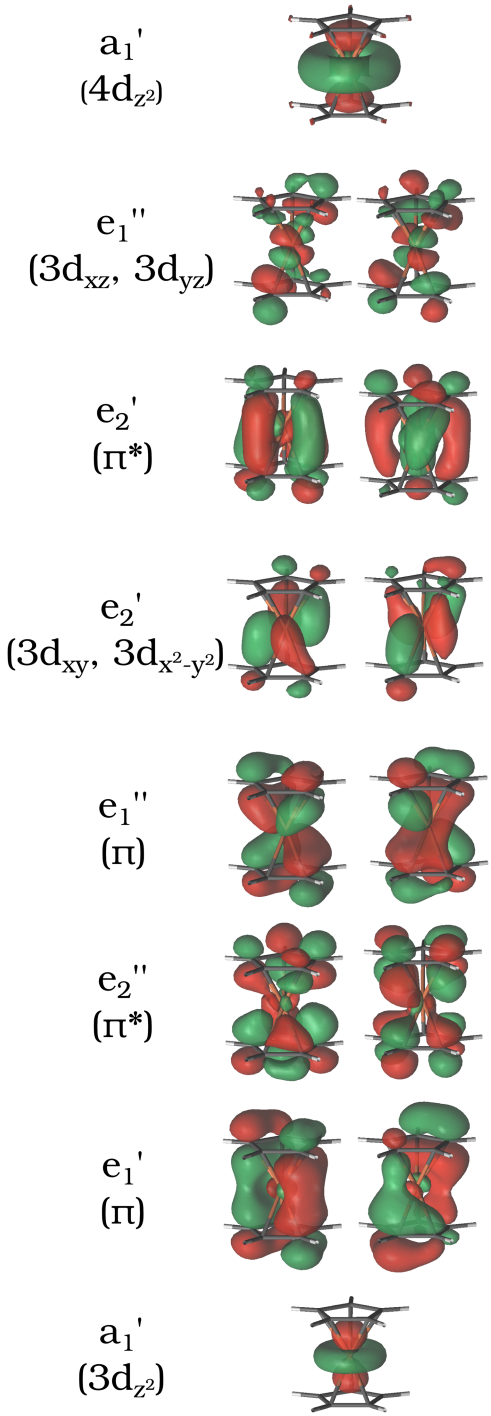

FIG. 2. Orbitals used in the (14,14) active space employed for ferrocene. All calculations were performed with C_1 symmetry; however, the orbitals are labeled according to their D_{5h} point-group designations.

For the ferrocene system, we calculate the CPC energy as

$$\Delta E_{CPC/f} = 2\left[E^{FeCp_2}_{FeCp_2}\left(Cp^-\right) - E^{Cp^-}_{FeCp_2}\left(Cp^-\right)\right] + E^{FeCp_2}\left(Fe^{2+}\right) - E^{Fe^{2+}}\left(Fe^{2+}\right), \tag{26}$$

where the subscripts indicate that the fragment geometry in the bound system is used (for the case of molecules) and the superscripts indicate which basis set is used.

IV. RESULTS

A. Separated H_2 molecules

In order to illustrate the performance of the CAS-PDFT method in terms of memory and timings, a series of calculations was performed on n non-interacting hydrogen molecules. Two electrons and two orbitals were included in the active space for each hydrogen molecule, generating an overall active space of $(2n, 2n)$.

A comparison of timings between CAS-PDFT, CASSCF, and CASPT2 is presented in Figure 3. The timings displayed for the CAS-PDFT and CASPT2 are cumulative, containing the time consumed for both the post-SCF step and the CASSCF calculation. Across all active space sizes, the cost of the calculation of the CAS-PDFT energy is only marginally higher than the time spent in the CASSCF calculation. In contrast, CASPT2 requires a significant amount of additional time for large active-space systems. This becomes quite apparent when the active space size is larger than (12,12). The time spent during a CASPT2 calculation can be segmented into three tasks: (i) transformation of the integrals from an atomic-orbital to a molecular-orbital basis (for all correlated molecular orbitals in the system), (ii) assembly of the three- and four-body density matrices from the CI coefficients, and (iii) solving the CASPT2 equations. CAS-PDFT, in contrast, reuses the integral transformation and the one- and two-body density matrices from the CASSCF wave function, resulting in a significant decrease

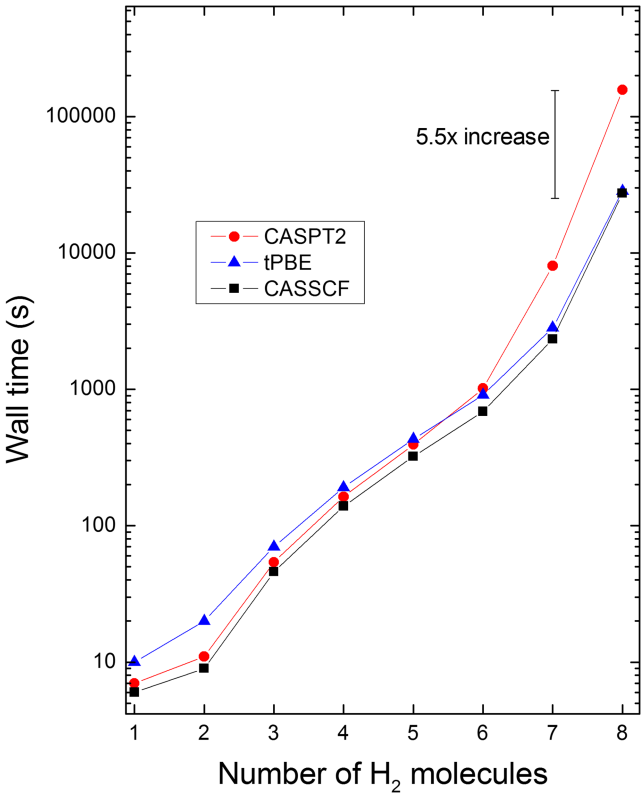

FIG. 3. Timing information for calculations on hydrogen molecule systems. A $(2n,2n)$ active space, where n is the number of hydrogen molecules, is used. The MC-PDFT and CASPT2 times are cumulative, containing both the time used to calculate the MCSCF wave function and the time used during the post-SCF step. The cc-pVQZ basis set was used.

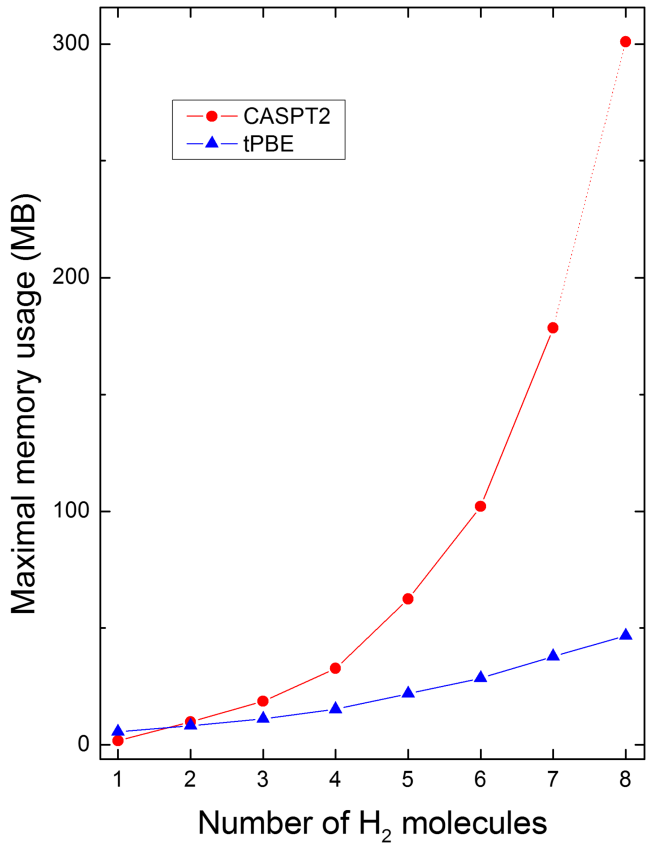

FIG. 4. Maximum-observed memory allocation for calculations on hydrogen molecule systems. A $(2n,2n)$ active space, where n is the number of hydrogen molecules, is used. The values do not include memory used during integral transformations (CASPT2, tPBE) or construction of higher-order density matrices (CASPT2). The $n = 8$ point of CASPT2 is estimated.

in time relative to CASPT2 for calculations involving large basis sets or large active spaces.

Information on the memory usage for both CAS-PDFT and CASPT2 is given in Figure 4. For CASPT2, we display only the maximum memory used while solving of the CASPT2 equations. This is considerably smaller than the memory used in both the integral transformation step and the building of the higher-order density matrices. In fact, these steps often have the largest memory footprint, and the construction of the higher-order density matrices is a bottleneck for large active space calculations. The performance of these steps is influenced by the supply of available memory—the fastest performance is achieved when all CI coefficients, density matrices, and intermediates (for the case of density matrix construction) or integrals, orbital coefficients, and intermediates (for integral transformations) can be held simultaneously in memory. Often, it is not possible to keep the CI coefficients and intermediate density matrix elements or partially transformed integrals in memory, and writing such data to files increases the computational time. Because the amount of memory depends strongly on the computer resources available, we have excluded these steps from the memory profiling. Even so, the memory costs are lower for CAS-PDFT for all except the smallest active spaces, and the scaling of CAS-PDFT is significantly lower than the scaling of CASPT2. The $n = 8$ point for CASPT2 in the figure is an estimate, as the time required for the calculation was too large for the use of memory-profiling tools.

TABLE I. Binding energy and dissociation enthalpy of ferrocene. Units are in kcal/mol.

	Without diffuse functions				With diffuse functions			
	CASSCF	CASPT2	tPBE	PBE	CASSCF	CASPT2	tPBE	PBE
	Basis I[a]				Basis II[b]			
D_e	591.7	674.3	670.4	716.4	574.1	652.7	648.7	694.7
ΔE_{ZPE}[c] + $\Delta E_{thermal}$[c]	−6.8	−6.8	−6.8	−6.8	−6.8	−6.8	−6.8	−6.8
ΔH°_{298}	584.9	667.5	663.6	709.6	567.3	645.9	641.9	709.6
Error[f]	−50.1	32.5	28.6	74.6	−67.7	10.9	6.9	74.6
	Basis III[d]				Basis IV[e]			
D	583.4	665.2	656.3	701.3	572.1	655.6	646.8	690.0
ΔE_{ZPE}[c] + $\Delta E_{thermal}$[c]	−6.8	−6.8	−6.8	−6.8	−6.8	−6.8	−6.8	−6.8
ΔH°_{298}	576.6	658.4	649.5	694.5	565.3	648.8	640.0	684.0
Error[f]	−58.4	23.4	14.5	59.5	−69.7	13.8	5.0	49.0

[a]C, H: cc-pVDZ-DK; Fe: cc-pVTZ-DK.
[b]C, H: maug-cc-pVDZ-DK; Fe: maug-cc-pVTZ-DK.
[c]From PBE0 with C, H: def2-TZVP; Fe: def2-QZVPP. Taken from Ref. 48.
[d]C, H: cc-pVTZ-DK; Fe: cc-pVQZ-DK.
[e]C, H: maug-cc-pVTZ-DK; Fe: maug-cc-pVQZ-DK.
[f]The experimental value, 635 ± 6 kcal/mol, is taken from Ref. 41.

B. Binding energy of ferrocene

We present the calculated heterolytic dissociation enthalpy of ferrocene in Table I, and we explore counterpoise correction (CPC) options in Table II. The table shows that KS-DFT with the PBE exchange-correlation functional overestimates the experimentally determined dissociation enthalpy with all four basis sets, whereas CASSCF underestimates the dissociation enthalpy by a large amount (>65 kcal/mol) with all four basis sets. The large underestimation by CASSCF shows that the inclusion of dynamic correlation energy is very important for a proper description of the dissociation enthalpy.

We consider first the results obtained without the application of the counterpoise correction. The selection of the basis set has a large impact on the quality of the results. For basis I, the smallest basis set employed, we find that CASPT2 and tPBE differ by approximately 4 kcal/mol, and both results are significantly higher than the experimental value. With minimal augmentation by diffuse functions (basis II), the calculated results agree more closely with the experimental value, with energy errors of 10.9 kcal/mol and 6.9 kcal/mol for CASPT2 and tPBE, respectively. When we repeat the calculations with larger basis sets, we obtain similar trends. Without diffuse functions (basis III), the heterolytic dissociation enthalpy for both methods is higher than the experimental value, although the results have improved when compared to basis I. Similarly, the addition of diffuse functions in basis IV reduces the difference between the experimental and calculated values. The CASPT2 result has an error of 13.8 kcal/mol, which is a larger error than was obtained with the smaller augmented basis set. In contrast, the tPBE result had an error of 5 kcal/mol, which is within the experimental uncertainty. This agrees well with

TABLE II. Bond dissociation enthalpy–counterpoise correction in kcal/mol. Results are compared to the experimental value of 635 ± 6 kcal/mol.[41]

	Without diffuse functions				With diffuse functions			
	CASSCF	CASPT2	tPBE	PBE	CASSCF	CASPT2	tPBE	PBE
	Basis I				Basis II			
ΔE_{CPC}	−15.3	−31.3	−12.1	−15.1	−3.0	−21.4	−2.3	−4.2
$\Delta H^\circ_{298,CPC-f}$[a]	569.6	636.2	651.5	701.3	564.3	624.6	639.5	690.5
$\Delta H^\circ_{298,CPC/2}$[b]	577.3	651.8	657.5	708.8	565.8	635.3	640.7	692.6
$Error_{CPC-f}$[a]	−65.4	1.2	16.5	66.3	−70.7	−10.4	4.5	55.5
$Error_{CPC/2}$[b]	−57.7	16.8	22.5	74.6	−69.2	0.3	5.7	57.6
	Basis III				Basis IV			
ΔE_{CPC}	−11.0	−14.3	−6.0	−7.3	−3.0	−9.2	−1.0	−1.2
$\Delta H^\circ_{298,CPC-f}$[a]	565.6	644.1	643.4	694.0	562.3	639.7	639.0	689.7
$\Delta H^\circ_{298,CPC/2}$[b]	571.1	651.2	646.5	697.7	563.8	644.3	639.5	690.3
$Error_{CPC-f}$[a]	−69.4	9.1	8.4	59.0	−72.7	4.7	4.0	54.7
$Error_{CPC/2}$[b]	−63.9	16.2	11.5	62.7	−71.2	9.3	4.5	55.3

[a]CPC–f: ΔE_{CPC} is added to ΔH°_{298}.
[b]CPC/2: $\Delta E_{CPC}/2$ is added to ΔH°_{298}.

TABLE III. Measured wall times in the calculation of the ferrocene energy with a (14,14) active space. Times are given in seconds.

	CASPT2	tPBE	CASPT2	tPBE
	Basis I		Basis II	
Reference wave function	7980	7980	17400	17400
Approx. time/SCF iteration[a]	235	235	483	483
Post-SCF	5220	231	9120	508
	Basis III		Basis IV	
Reference wave function	8160	8160	22080	22080
Approx. time/SCF iteration[a]	249	249	414	414
Post-SCF	6120	305	10320	664

[a]CPC–f: ΔE_{CPC} is added to ΔH°_{298}.

the value reported by Phung, Vancoille, and Pierloot using RASPT2 (4.1 kcal/mol error) with a larger (18,18) active space, a much larger basis set, and slightly different geometries.

Next, we consider the effect of adding a CPC to account for BSSE. Two different CPC prescriptions were used: the addition of the entire ΔE_{CPC} to ΔH°_{298} (labeled CPC-f) and the addition of one-half of ΔE_{CPC} to ΔH°_{298} (labeled CPC/2). When either CPC prescription is used, the magnitude of the CASSCF error always shows an increase, and the magnitudes of the CASPT2 and tPBE errors always decrease. CASPT2 exhibits a very large ΔE_{CPC}, and a single CPC prescription does not give consistently better results. Especially large differences are seen with the smaller basis sets (I and II), where ΔE_{CPC} is largest. In contrast, tPBE exhibits a much smaller ΔE_{CPC}; one sees the following trend in the magnitudes of ΔE_{CPC} for the multireference methods: CASPT2 > CASSCF > tPBE. The smaller BSSE uncertainty in density functional theory is one of its advantages over wave function theory. Use of the augmented bases (II and IV) with either CPC prescription (CPC-f or CPC/2) gave tPBE results that agree with the experimental heterolytic dissociation enthalpy within the experimental uncertainty. In fact, the tPBE results obtained with the smaller basis set (II) are nearly identical to the results obtained with the larger basis set (IV); this is very encouraging.

We present wall timings for the calculation of the energy of $FeCp_2$ in Table III. For the (14,14) active space used, the CASSCF calculation is the largest contributor to the total time. This is partially because the CASSCF calculation consists of multiple self-consistency iterations (typically 30-40). A comparison of the post-SCF step timings shows a striking difference between the CASPT2 and tPBE. The time needed for the tPBE post-SCF step is very similar to the time needed for a single CASSCF iteration. On the other hand, the CASPT2 post-SCF step requires significantly more time—for this active space selection, making CASPT2 over an order of magnitude more expensive. For larger active spaces, we expect an even more pronounced difference.

V. DISCUSSION

The results from the H_2 molecule highlight the differences in memory and timing requirements between CAS-PDFT and CASPT2. Extensive profiling of the algorithm has shown that the most time-consuming steps in a CAS-PDFT calculation are the transformation of the atomic orbitals to the molecular orbitals on the density functional grid, the calculation of the on-top pair density on the density functional grid, and the evaluation of the translated functional. In addition, a limited integral transformation is performed, transforming the four-index electron repulsion integrals (ERIs) in the AO basis to a limited subset of ERIs in the MO basis (the set containing three active orbital indices and one general orbital index). This is identical to the integral transform that is done in the CASSCF calculation, so if the integrals have been saved, this step need not be repeated. In any case, this step is generally quite inexpensive. The net result of all steps is that the time needed for a CAS-PDFT calculation is comparable to the time needed for a single CASSCF iteration. CASPT2, on the other hand, requires a much more significant time investment. An integral transformation must be performed over the entire CASPT2 interaction space which contains inactive, active, and virtual orbitals. While this scales as the fifth power of the number of interacting MOs, for large basis set calculations, this step can become quite costly. In addition, the CASPT2 method requires higher order density matrices that must be constructed from the CI coefficients from the CASSCF calculation. When the active space becomes large, the number of CI coefficients increases dramatically, resulting in a very large time needed to calculate the three- and four-body density matrix elements. The CAS-PDFT method, in contrast, only requires the 2-body density matrix, which is already available from the CASSCF calculation. Finally, solving the CASPT2 equations takes significant time as the size of the system increases. We see a dramatic difference in post-SCF computation time, especially when the active space size approaches or exceeds (12,12). For smaller active spaces, CASPT2 and CAS-PDFT often have similarly small timings. For cases with large numbers of inactive (doubly occupied) orbitals, we expect the timing differences to be even larger because the contribution to the density and on-top pair density by the inactive orbitals, as required by CAS-PDFT, is much simpler to calculate than the explicit correlation of these orbitals in CASPT2. We see these increased time differences illustrated in the ferrocene timing information (Table III).

The calculation of the dissociation enthalpy of ferrocene demonstrates that CAS-PDFT can provide results within experimental accuracy at a significantly lower post-SCF cost than CASPT2. With minimally augmented basis sets the tPBE method was both accurate and stable to changes in the basis set size. There is not a uniform agreement on a CPC prescription to account for BSSE. Several authors have advocated for the scaling of the CPC by one-half[64–66] to balance the competing errors due to BSSE and due to basis set incompleteness. With CASPT2, our results have shown that the choice of one prescription over another can result in very large differences in the heterolytic dissociation enthalpy, especially in the case of smaller basis set choices where ΔE_{CPC} is large. In contrast, this dispute on whether to use full, half, or no CPC can largely be ignored for the CAS-PDFT results. The ΔE_{CPC} obtained from tPBE, most notably in the cases of diffuse basis sets, was so small that either prescription (or even total neglect of the CPC)

results in a heterolytic dissociation enthalpy that is within (or very near) the uncertainty in the experimental value. We find very good agreement between CASPT2, tPBE, and experiment for the largest basis set used (IV) with the full CPC-f correction applied.

The use of CASSCF limits the size of systems that can be studied with both CASPT2 and MC-PDFT. Larger active-space systems can be studied by using RAS or GAS[28] wave functions, which limit the number of CI coefficients in the wave function expansion. The size of the active space limits the usefulness of PT2 theories because they require the three- and four-body reduced density matrices whose size scales as N^6 and N^8, respectively. On the other hand, MC-PDFT theory has no dependence on CI coefficients nor does it depend on matrices larger than the two-body reduced density matrix. This theoretically allows for MC-PDFT to use reference wave functions with more than 100 active orbitals.

VI. CONCLUDING REMARKS

MC-PDFT is a very attractive tool for theoretical chemistry as it provides a low-cost way to add dynamic correlation energy to multireference wave function methods. In this work we have presented the algorithm used in the MC-PDFT method. We have discussed how its low scaling (N^4 in the number of active orbitals) allows the use of large active spaces even in situations where other post-SCF methods become cost prohibitive.

In the determination of the heterolytic dissociation enthalpy of ferrocene, even though the post-SCF step of CAS-PDFT calculations was 15-20 times faster than CASPT2 ones, there was no reduction in accuracy. In fact, the results obtained with the tPBE functional are within the accuracy of the experimental value and less susceptible to errors associated with basis set choice or basis set superposition error.

These results are quite encouraging for the application of MC-PDFT theory to large active space systems. We are currently working on the application of MC-PDFT methods to GASSCF wave functions with more than 40 active orbitals.

SUPPLEMENTARY MATERIAL

See supplementary material for coordinates and absolute energies for heterolytic dissociation energy of ferrocene.

ACKNOWLEDGMENTS

This work was supported in part by the National Science Foundation by Grant No. CHE14-64536.

[1]M. S. Gordon and M. W. Schmidt, in *Applications of Computational Chemistry: The First Forty Years*, edited by C. E. Dykstra, G. Frenking, K. S. Kim, and G. E. Scuseria (Elsevier, Amsterdam, 2005), pp. 1167–1189.
[2]H. Nakano, T. Nakajima, T. Tsuneda, and K. Hirao, in *Applications of Computational Chemistry: The First Forty Years*, edited by C. E. Dykstra, G. Frenking, K. S. Kim, and G. E. Scuseria (Elsevier, Amsterdam, 2005), pp. 507–557.
[3]B. O. Roos, in *Applications of Computational Chemistry: The First Forty Years*, edited by C. E. Dykstra, G. Frenking, K. S. Kim, and G. E. Scuseria (Elsevier, Amsterdam, 2005), pp. 725–764.
[4]T. Schwabe and S. Grimme, Acc. Chem. Res. **41**, 569 (2008).
[5]T. Yamashita, Y. Peng, C. Knight, and G. A. Voth, J. Chem. Theory Comput. **8**, 4863 (2012).
[6]F. Aquilante, J. Autschbach, R. K. Carlson, L. F. Chibotaru, M. G. Delcey, L. De Vico, I. F. Galván, N. Ferr, L. M. Frutos, L. Gagliardi, M. Garavelli, A. Giussani, C. E. Hoyer, G. Li Manni, H. Lischka, D. Ma, P.-Å. Malmqvist, T. Müller, A. Nenov, M. Olivucci, T. B. Pedersen, D. Peng, F. Plasser, B. Pritchard, M. Reiher, I. Rivalta, I. Schapiro, J. Segarra-Mart, M. Stenrup, D. G. Truhlar, L. Ungur, A. Valentini, S. Vancoillie, V. Veryazov, V. P. Vysotskiy, O. Weingart, F. Zapata, and R. Lindh, J. Comput. Chem. **37**, 506 (2016).
[7]C. D. Sherrill and P. Piecuch, J. Chem. Phys. **122**, 124104 (2005).
[8]Y. Zhao, O. Tishchenko, J. R. Gour, W. Li, J. J. Lutz, P. Piecuch, and D. J. Truhlar, J. Phys. Chem. A **113**, 5786 (2009).
[9]P. G. Szalay, T. Müller, G. Gidofalvi, H. Lischka, and R. Shepard, Chem. Rev. **112**, 108 (2011).
[10]D. I. Lyakh, M. Musiał, V. F. Lotrich, and R. J. Bartlett, Chem. Rev. **112**, 182 (2012).
[11]X. Li and J. Paldus, J. Chem. Phys. **108**, 637 (1998).
[12]S. Das, D. Datta, R. Maitra, and D. Mukherjee, Chem. Phys. **349**, 115 (2008).
[13]G. Li Manni, R. K. Carlson, S. Luo, D. Ma, J. Olsen, D. G. Truhlar, and L. Gagliardi, J. Chem. Theory Comput. **10**, 3669 (2014).
[14]D. Ma, G. Li Manni, and L. Gagliardi, J. Chem. Phys. **135**, 044128 (2011).
[15]P.-Å. Malmqvist, A. Rendell, and B. Roos, J. Phys. Chem. **94**, 5477 (1990).
[16]J. Ivanic, J. Chem. Phys. **119**, 9364 (2003).
[17]G. Li Manni, D. Ma, F. Aquilante, J. Olsen, and L. Gagliardi, J. Chem. Theory Comput. **9**, 3375 (2013).
[18]G. Li Manni, F. Aquilante, and L. Gagliardi, J. Chem. Phys. **134**, 034114 (2011).
[19]G. Li Manni, S. D. Smart, and A. Alavi, J. Chem. Theory Comput. **12**, 1245 (2016).
[20]G. K.-L. Chan and S. Sharma, Annu. Rev. Phys. Chem. **62**, 465 (2011).
[21]Y. Kurashige, Mol. Phys. **112**, 1485 (2014).
[22]Y. Kurashige and T. Yanai, J. Chem. Phys. **135**, 094104 (2011).
[23]D. A. Mazziotti, Chem. Rev. **112**, 244 (2012).
[24]J. Fosso-Tande, D. R. Nascimento, and A. E. DePrince III, Mol. Phys. **114**, 423 (2015).
[25]A. W. Schlimgen,C. W. Heaps, and D. A. Mazziotti, J. Phys. Chem. Lett. **7**, 627 (2016).
[26]K. Andersson, P.-Å. Malmqvist, B. O. Roos, A. J. Sadlej, and K. Wolinski, J. Phys. Chem. **94**, 5483 (1990).
[27]P.-Å. Malmqvist, K. Pierloot, A. R. M. Shahi, C. J. Cramer, and L. Gagliardi, J. Chem. Phys. **128**, 204109 (2008).
[28]D. Ma, G. Li Manni, J. Olsen, and L. Gagliardi, J. Chem. Theory Comput. **12**, 3208 (2016).
[29]C. Angeli, R. Cimiraglia, and J.-P. Malrieu, Chem. Phys. Lett. **350**, 297 (2001).
[30]C. Angeli, M. Pastore, and R. Cimiraglia, Theor. Chem. Acc. **117**, 743 (2006).
[31]R. K. Carlson, G. Li Manni, A. L. Sonnenberger, D. G. Truhlar, and L. Gagliardi, J. Chem. Theory Comput. **11**, 82 (2015).
[32]C. E. Hoyer, S. Ghosh, D. G. Truhlar, and L. Gagliardi, J. Phys. Chem. Lett. **7**, 586 (2016).
[33]C. E. Hoyer, L. Gagliardi, and D. G. Truhlar, J. Phys. Chem. Lett. **6**, 4184 (2015).
[34]R. K. Carlson, D. G. Truhlar, and L. Gagliardi, J. Chem. Theory Comput. **11**, 4077 (2015).
[35]S. O. Odoh, G. Li Manni, R. K. Carlson, D. G. Truhlar, and L. Gagliardi, Chem. Sci. **7**, 2399 (2016).
[36]E. Fromager, S. Knecht, and H. J. A. Jensen, J. Chem. Phys. **138**, 084101 (2013).
[37]M. Hubert, E. D. Hedegård, and H. J. A. Jensen, J. Chem. Theory Comput. **12**, 2203 (2016).
[38]M. Hubert, H. J. A. Jensen, and E. D. Hedegård, J. Phys. Chem. A **120**, 36 (2016).
[39]E. D. Hedegård, S. Knecht, J. S. Kielberg, H. J. A. Jensen, and M. Reiher, J. Chem. Phys. **142**, 224108 (2015).
[40]A. J. Garza, I. W. Bulik, T. M. Henderson, and G. E. Scuseria, J. Chem. Phys. **142**, 044109 (2015).
[41]M. F. Ryan, J. R. Eyler, and D. E. Richardson, J. Am. Chem. Soc. **114**, 8611 (1992).
[42]K. Pierloot, B. J. Persson, and B. O. Roos, J. Phys. Chem. **99**, 3465 (1995).

[43]S. Coriani, A. Haaland, T. Helgaker, and P. Jorgensen, ChemPhysChem **7**, 245 (2006).
[44]J. Frunzke, M. Lein, and G. Frenking, Organometallics **21**, 3351 (2002).
[45]F. Furche and J. P. Perdew, J. Chem. Phys. **124**, 044103 (2006).
[46]E. J. Padma Malar, Eur. J. Inorg. Chem. **13**, 2723 (2004).
[47]M. Swart, Inorg. Chim. Acta **360**, 179 (2007).
[48]S. Vancoillie, H. Zhao, V. T. Tran, M. F. A. Hendrickx, and K. Pierloot, J. Chem. Theory Comput. **7**, 3961 (2011).
[49]Q. M. Phung, S. Vancoillie, and K. Pierloot, J. Chem. Theory Comput. **8**, 883 (2012).
[50]C. J. Stein, V. von Burg, and M. Reiher, J. Chem. Theory Comput. **12**, 3764 (2016).
[51]B. O. Roos, P. R. Taylor, and P. E. M. Siegbahn, Chem. Phys. **48**, 157 (1980).
[52]T. H. Dunning, Jr., J. Chem. Phys. **90**, 1007 (1989).
[53]P. Piecuch, S. A. Kucharski, K. Kowalski, and M. Musial, Comput. Phys. Commun. **149**, 71 (2002).
[54]A. Schaefer, C. Huber, and R. Ahlrichs, J. Chem. Phys. **100**, 5829 (1994).
[55]B. A. Hess, Phys. Rev. A **33**, 3742 (1986).
[56]M. W. Schmidt, K. K. Baldridge, J. A. Boatz, S. T. Elbert, M. S. Gordon, J. H. Jensen, S. Koseki, N. Matsunaga, K. A. Nguyen, S. Su, T. L. Windus, M. Dupuis, and J. A. Montgomery, J. Comput. Chem. **14**, 1347 (1993).
[57]R. A. Kendall, T. H. Dunning, Jr., and R. J. Harrison, J. Chem. Phys. **96**, 6796 (1992).
[58]N. B. Balabanov and K. A. Peterson, J. Chem. Phys. **123**, 064107 (2005).
[59]E. Papajak, H. R. Leverentz, J. Zheng, and D. G. Truhlar, J. Chem. Theory Comput. **5**, 1197 (2009).
[60]E. Papajak and D. G. Truhlar, J. Chem. Theory Comput. **6**, 597 (2010).
[61]F. Aquilante, T. B. Pedersen, and R. Lindh, J. Chem. Phys. **126**, 194106 (2007).
[62]S. F. Boys and F. Bernardi, Mol. Phys. **100**, 65 (2002).
[63]F. B. van Duijneveldt, J. G. C. M. van Duijneveldt-van de Rijdt, and J. H. van Lenthe, Chem. Rev. **94**, 1873 (1994).
[64]T. Schwabe and S. Grimme, Phys. Chem. Chem. Phys. **9**, 3397 (2007).
[65]L. A. Burns, M. S. Marshall, and C. D. Sherrill, J. Chem. Theory Comput. **10**, 49 (2014).
[66]B. Brauer, M. K. Kesharwani, and J. M. L. Martin, J. Chem. Theory Comput. **10**, 3791 (2014).